Electronic Supplementary Material (ESI) for Journal of Materials Chemistry A.

Isomerism effect on the photovoltaic properties of benzotrithiophene-based hole-transporting materials

Inés García-Benito,[a] Iwan Zimmermann,[b] Javier Urieta-Mora,[c] Juan Aragó,[d] Agustín Molina-Ontoria,[a] Enrique Ortí,[d] Nazario Martín,[a,c]* Mohammad Khaja Nazeeruddin[b]**

[a] *IMDEA Nanociencia, Cantoblanco, 28049 Madrid, Spain.*
[b] *Group for Molecular Engineering of Functional Materials and Laboratory for Photonics and Interfaces, EPFL VALAIS, CH-1951 Sion, Switzerland.*
[c] *Departamento Química Orgánica, Facultad C. C. Químicas, Universidad Complutense de Madrid, Av. Complutense s/n, 28040 Madrid, Spain.*
[d] *Instituto de Ciencia Molecular, Universidad de Valencia, Catedrático José Beltrán 2, 46980 Paterna, Spain.*

TABLE OF CONTENTS

1. Experimental

General Methods. Chemicals and reagents were purchased from commercial suppliers and used as received. All solvents were dried according to standard procedures. Air-sensitive reactions were carried out under argon atmosphere. The device preparation was done in a glovebox under nitrogen atmosphere. Flash chromatography was performed using silica gel (Merck, Kieselgel 60, 230-240 mesh or Scharlau 60, 230-240 mesh). Analytical thin layer chromatography (TLC) was performed using aluminum-coated Merck Kieselgel 60 F254 plates. NMR spectra were recorded on a Bruker Advance 300 (^{1}H: 400 MHz; ^{13}C: 101 MHz) spectrometer at 298 K using partially deuterated solvents as internal standards. Coupling constants (*J*) are denoted in Hz and chemical shifts (δ) in ppm. Multiplicities are denoted as follows: s = singlet, d = doublet, t = triplet, m = multiplet. FT-IR spectra were recorded on a Bruker Tensor 27 (ATR device) spectrometer. UV-Vis spectra were recorded in a Varian Cary 50 spectrophotometer. Mass spectra, Matrix-assisted, Laser desorption ionization (coupled to a Time-of-Flight analyzer) experiments (MALDI-TOF) were recorded on a MAT 95 thermo spectrometer and a Bruker REFLEX spectrometer, respectively. Cyclic voltammetry (CV) experiments were conducted in 0.1 M solution of $^{n}Bu_4PF_6$ in dichloromethane (DCM). Glassy carbon was used as working electrode and platinum wires were used as counter and reference electrodes. Before each measurement, solutions were deoxygenated with N_2. Ferrocene was added as an internal standard; its oxidation potential in DCM was positioned at 0.7 V vs. normal hydrogen electrode (NHE) and HTMs' oxidation potentials were recalculated in reference to NHE. Thermogravimetric analysis (TGA) was performed using a TA Instruments TGAQ500 with a ramp of 10 °C/min under N_2 from 100 to 1000 °C. Differential scanning calorimetry (DSC) was run on a Discovery DSC from TA instruments. Three cycles were recorded under nitrogen, heating (until 400 °C) and cooling (50 °C) at 20 °C/min of scanning rate.

2. Synthetic details and characterization

Compounds **1**, **2, 4** and **5** were prepared according to previously reported synthetic procedures (see: a) *J. Org. Chem.,* **1989***, 54,* 4203–4205; b) *Org. Lett.* **2011**, *13*, 6062–6065) and showed identical spectroscopic properties to those reported therein.

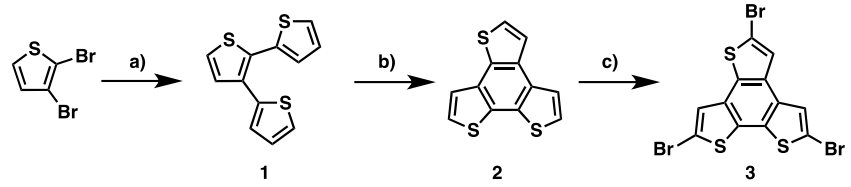

Scheme S1. *Reagents and conditions: a) 2-(tributylstannyl)thiophene, $Pd(PPh_3)_2Cl_2$, DMF, 130 ℃, 89 %; b) I_2, PhMe, hv, 76 %; c) NBS, CH_3Cl:AcOH (2:1), 70 ℃, 65 %.*

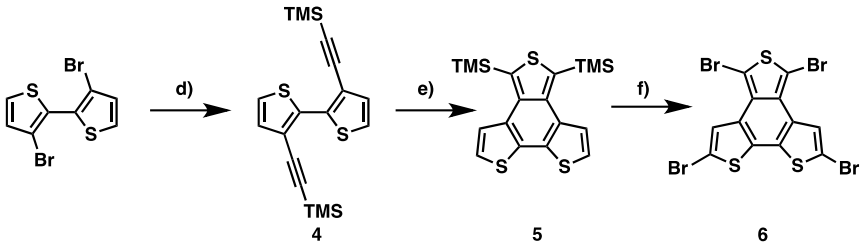

Scheme S2. *Reagents and conditions: d) TMSA, $Pd(PPh3)_2Cl_2$, CuI, DIPA, 80 ℃; e) S_8, $Rh(PPh_3)_3Cl$, benzene, 80 ℃, N_2; f) NBS, CH_3Cl:AcOH (2:1), 70 ℃, 57 %.*

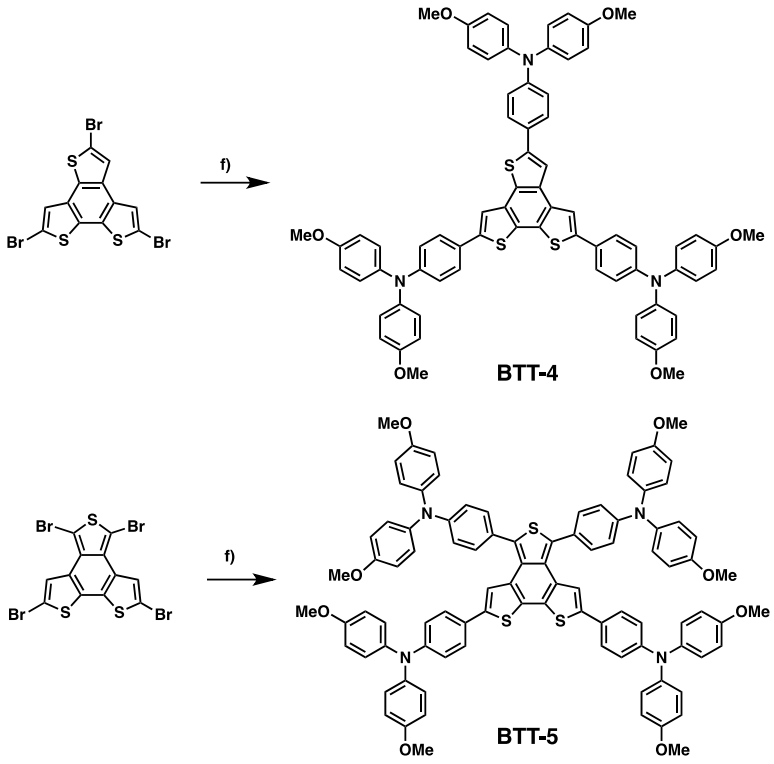

Scheme S3. *Reagents and conditions: f) 4-(4,4,5,5-tetramethyl-1,3,2-dioxaborolan-2-yl)-N,N-bis(4-methoxyphenyl)aniline, $Pd(PPh_3)_4$, K_3PO_4, DMF.*

2,5,8-Tribromobenzo[1,2-*b*:3,4-*b*':6,5-*b*'']trithiophene (3)

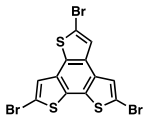

NBS (1.51 g, 8.53 mmol) was added portionwise to a solution of benzo[1,2-*b*:3,4-*b*':6,5-*b*'']trithiophene (**2**) (500 mg, 2.03 mmol) in a mixture of chloroform and acetic acid (2:1) (15 mL) under light exclusion conditions. The reaction was then heated to reflux under nitrogen atmosphere. The resulting precipitate was filtered and washed with water, MeOH and chloroform to afford the tribromo derivative **3** in 65 % yield as a brown solid. ^{1}H NMR (400 MHz, DMSO-d_6) δ/ppm 8.29 (s, 1H), 8.26 (s, 1H), 8.10 (s, 1H). Given the low solubility of this compound ^{13}C NMR was not possible. MALDI for $C_{12}H_3Br_3S_3$ [M$^+$] 483.1.

2,4,6,8-Tetrabromobenzo[1,2-*b*:6,5-*b*':3,4-*c*'']trithiophene (6)

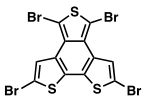

NBS (394 mg, 2.2 mmol) was added portionwise to a solution of 4,6-bis(trimethylsilyl)benzo[1,2-*b*:6,5-*b*':3,4-*c*'']trithiophene (**5**) (173 mg, 0.44 mmol) in a mixture of chloroform and acetic acid (2:1) (15 mL) under light exclusion conditions. The reaction was then heated to reflux under nitrogen atmosphere. The resulting precipitate was filtered and washed with water, MeOH and chloroform to afford the tetrabromo derivative **6** in 57 % yield as a brownish solid. Given the low solubility of this compound. ^{1}H NMR and ^{13}C NMR were not possible. MALDI for $C_{12}H_2Br_4S_3$ [M$^+$] 561.6

BTT-4

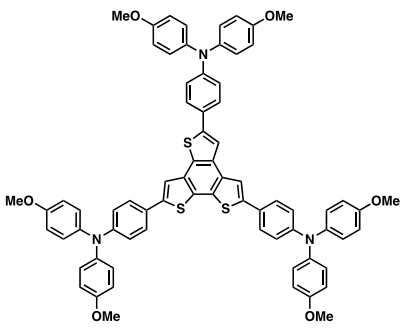

A solution of **3** (145 mg, 0.30 mmol), 4-(4,4,5,5-tetramethyl-1,3,2-dioxaborolan-2-yl)-N,N-bis(4-methoxyphenyl)aniline (453 mg, 1.05 mmol), K_3PO_4 (1.52 gr, 7.2 mmol) and $Pd(PPh_3)_4$ (70 mg, 0.06 mmol) in DMF (6 mL) was degassed for 30 minutes under nitrogen. The reaction was heated at 105 °C for 3 hours. The mixture was cooled to room temperature and water was added. The resulting precipitate was filtered and washed with water and dissolved in hot chloroform. The organic phase was dried over sodium sulfate. The solvent was removed under reduced pressure and the crude product was purified by flash column chromatography (silica gel, CH_2Cl_2 and then CH_2Cl_2:AcOEt (100:2)) to afford **BTT-4** as a yellow solid (233 mg, 0.25 mmol),

yield 67 %. ^{1}H NMR (400 MHz, THF) δ/ppm 8.04 (s, 1H), 8.03 (s, 1H), 7.78 (s, 1H), 7.64–7.60 (m, 6H), 7.10–7.06 (m, 12H), 6.95–6.93 (m, 6H), 6.89–6.85 (m, 12H), 3.77 (s, 18H); ^{13}C NMR (101 MHz, $CDCl_3$) δ/ppm 160.3, 160.2(2), 152.8, 152.6(2), 147.1, 146.5, 146.2, 144.1, 144.01, 143.9(2), 137.6, 137.3, 135.9, 133.9, 132.8, 131.8, 130.4(2), 130.3, 130.2, 130.1, 129.7, 129.5, 129.2, 123.6, 123.5, 123.4, 120.4(2), 119.4, 118.2, 58.2; FTIR (neat): 3035, 2996, 2832, 1600, 1503, 1318, 1282, 1239, 1034, 824 cm^{-1}; HRMS calcd for $C_{72}H_{57}N_3O_6S_3$ [M$^+$], 1155.3404; found 1155.3362.

BTT-5

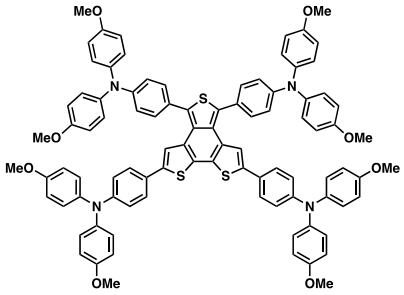

A solution of **6** (115 mg, 0.20 mmol), 4-(4,4,5,5-tetramethyl-1,3,2-dioxaborolan-2-yl)-N,N-bis(4-methoxyphenyl)aniline (397 mg, 0.92 mmol), K_3PO_4 (1.04 gr, 4.9 mmol) and $Pd(PPh_3)_4$ (47 mg, 0.04 mmol) in DMF (6 mL) was degassed for 30 minutes under nitrogen. The reaction was heated at 100 °C for 2 hours. The mixture was cooled to room temperature and water was added. The resulting precipitate was filtered and washed with water and dissolved in hot chloroform. The organic phase was dried over sodium sulfate. The solvent was removed under reduced pressure and the crude product was purified by flash column chromatography (silica gel, CH_2Cl_2 and then CH_2Cl_2:AcOEt (100:2)) to afford **BTT-5** as an orange solid (165 mg, 0.25 mmol), yield 56 %. ^{1}H NMR (400 MHz, THF) δ/ppm 7.44–7.41 (m, 4H), 7.38 (s, 2H), 7.37–7.34 (m, 4H), 7.14–7.06 (m, 16H), 7.05–7.02 (m, 4H), 6.97–6.93 (m, 4H), 6.91–6.86 (m, 8H), 6.84–6.80 (m, 8H), 3.77 (m, 4H), 3.72 (s, 12H); ^{13}C NMR (101 MHz, $CDCl_3$) δ/ppm 156.0, 148.9, 148.3, 140.7, 140.5, 133.3, 131.4, 130.3, 129.7, 126.7, 126.6, 126.4, 120.4, 120.0, 119.0, 114.8, 55.4(2); FTIR (neat): 3037, 2948, 2833, 1603, 1500, 1320, 1280, 1239, 1034, 824 cm^{-1}; HRMS calcd for $C_{92}H_{74}N_4O_8S_3$ [M$^+$], 1458.4663; found 1458.4706.

3. Computational Details

Quantum-chemical calculations were carried out with the Gaussian 09 (revision D.01) software package.[1] All the calculations were performed within the density functional theory (DFT) framework using the B3LYP functional[2] and the 6-31G** basis set.[3] Solvent effects were considered within the self-consistent reaction field (SCRF) theory by using the polarized continuum model (PCM) approach.[4] C_3, C_1 and C_2 symmetry constraints were imposed during the optimizations of **BTT-3**, **BTT-4** and **BTT-5**, respectively, whereas C_{3h}, C_s and C_{2v} constraints were used to calculate the respective **C-3**, **C-4** and **C-5** cores. The OMeTPA substituent and the *spiro*-OMeTAD reference molecule were also optimized under C_2 symmetry. Vertical electronic transition energies to the lowest-energy singlet excited states of **BTT-3**, **BTT-4** and **BTT-5** were computed by using the time-dependent density functional theory (TDDFT) approach.[5] The lowest 40 singlet excited states were calculated at the B3LYP/6-31G** level using the ground-state optimized geometries. Geometry optimizations of the radical cations of **BTT-3**, **BTT-4** and **BTT-5**, their isomeric BTT cores and *spiro*-OMeTAD were also performed to evaluate the reorganization energy (the evaluation process is explained below). Radical cations are treated as open-shell systems and computed within the spin-unrestricted DFT approximation at the UB3LYP/6-31G** level. Additionally, dication, trication and tetracation species were computed. Molecular orbitals were plotted using the Chemcraft 1.6 software with isovalue contours of ±0.03 a.u.[6]

Figure S1 shows the B3LYP/6-31G**-optimized values calculated for selected bond lengths of the BTT cores **C-3**, **C-4** and **C-5**, and their OMeTPA derivatives **BTT-3**, **BTT-4** and **BTT-5**. Figure S2 displays the optimized structures of the three BTT-based HTMs. For **BTT-3** and **BTT-4**, the BTT core preserves its planar structure and the phenyl rings connecting the peripheral OMeTPA groups are twisted by around 22–25° with respect to the plane defined by the core. Therefore, despite the bulky terminal OMeTPA groups, **BTT-3** and **BTT-4** exhibit quite planar structures that, in principle, can give rise to stacking aggregation in the solid state. In contrast, **BTT-5** presents a more crowded structure due to the presence of four OMeTPA arms. The steric interaction between the OMeTPA groups force the BTT core to slightly deviate from planarity, and now the dihedral angles formed by the phenyl rings connecting the OMeTPA groups and the BTT core are of 27.0° for the OMeTPA groups linked to the 2,2'-bithiophene unit and of 56.8° for the other two OMeTPA groups. The congested structure of **BTT-5** makes more difficult the aggregation in the solid state. Figure S3 depicts the topology and energy of

the frontier molecular orbitals participating in the electronic transitions to the lowest-energy singlet excited states.

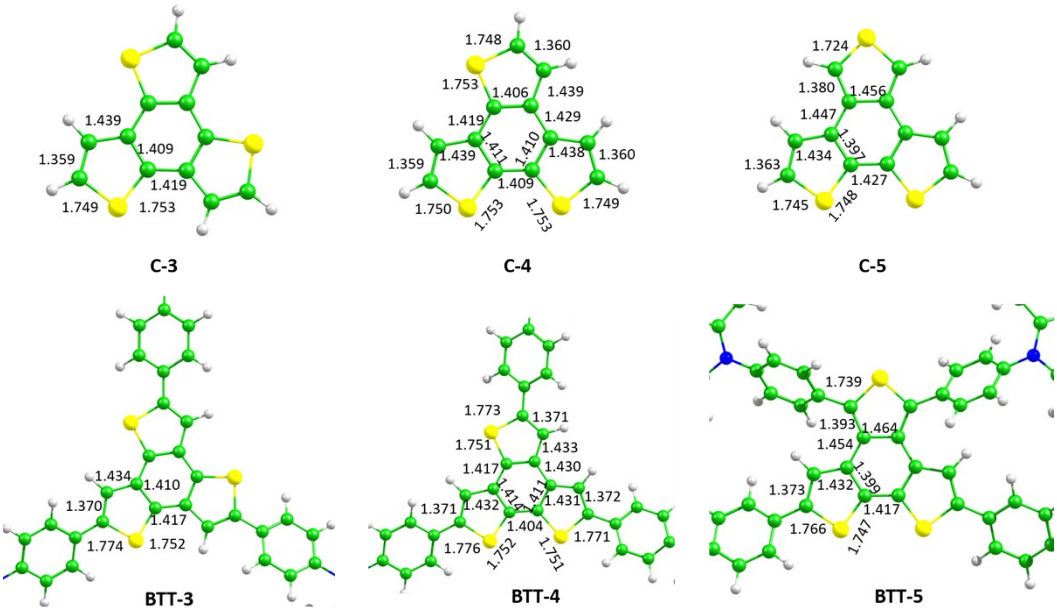

Figure S1. Optimized bond lengths (in Å) calculated at the B3LYP/6-31G** level, in CH_2Cl_2 solution, for the isomeric BTTs cores **C-3**, **C-4** and **C-5** and for the BTT-based derivatives **BTT-3**, **BTT-4** and **BTT-5**. For the latter, the terminal OMeTPA pendant groups have been partially omitted and only the bond lengths for the BTT cores are shown. Symmetry constraints were used for **C-3** (C_{3h}), **BTT-3** (C_3), **C-4** (C_s), **C-5** (C_{2v}) and **BTT-5** (C_2)**.**

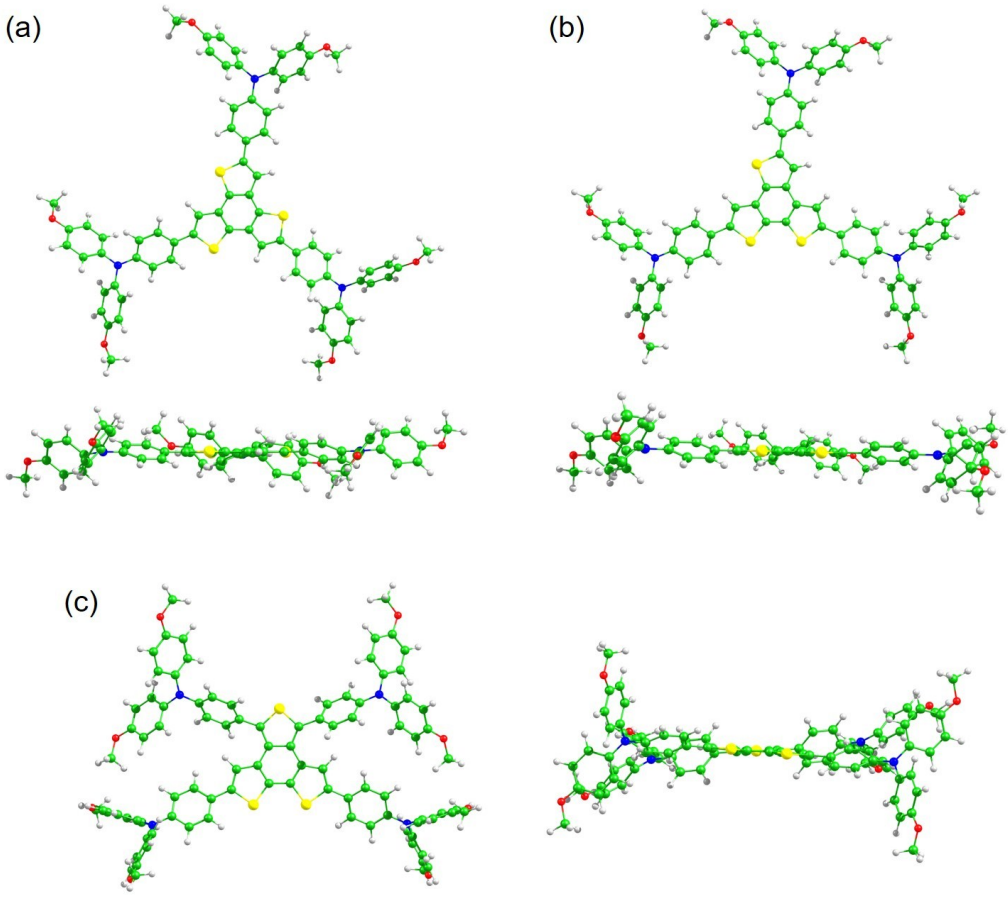

Figure S2. Top and side views of the minimum-energy optimized geometries calculated at the B3LYP/6-31G** level for **BTT-3** (a), **BTT-4** (b) and **BTT-5** (c).

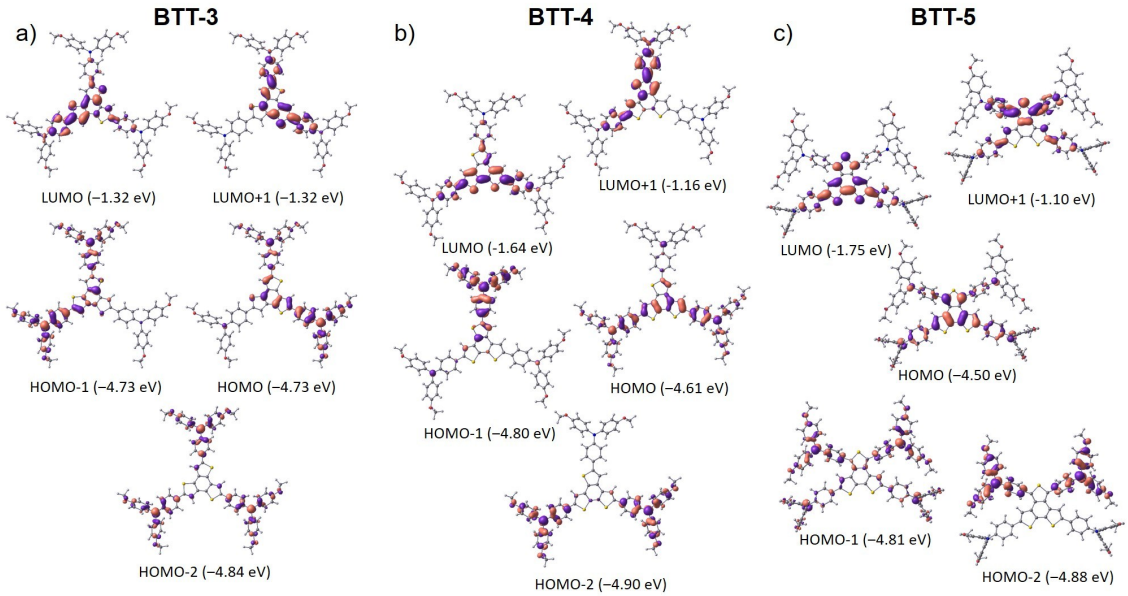

Figure S3. Isovalue contours (±0.03 a.u.) and energies calculated at the B3LYP/6-31G** level in CH_2Cl_2 for selected molecular orbitals of **BTT-3** (a), **BTT-4** (b) and **BTT-5** (c).

Oxidized species. B3LYP/6-31G** calculations in CH_2Cl_2 were used to investigate the molecular structure and the charge distribution of the BTT derivatives in different oxidation states, from the monocation to the trication; the tetracation was also computed for **BTT-5** Cation species were computed to be doublet open-shell species. For [**BTT-3**]$^{\bullet+}$, DFT calculations cannot deal with the degenerate doublet state that would result from the degenerate HOMO orbitals. Therefore, spin-unrestricted UB3LYP calculations break the molecular symmetry and lead to a nonsymmetric radical cation, in which the three constituting molecular fragments are slightly different. Dications of the BTT derivatives were calculated as singlet closed-shell species, in which both electrons are extracted from the same orbital, and triplet open-shell species, in which the electrons are extracted from different orbitals. For [**BTT-3**]$^{2+}$ and [**BTT-4**]$^{2+}$ the triplet state was found to be more stable than the singlet state by 0.35 eV and 0.14 eV, respectively. In contrast, the singlet state of [**BTT-5**]$^{2+}$ was calculated to be the most stable species by 0.10 eV. The different nature of the dication for **BTT-5** is due to the fact that the HOMO and HOMO-1 are separated by a larger energy difference of 0.31 eV (Figure S3). In the case of trications, doublet and quadruplet open-shell states were computed. For [**BTT-3**]$^{3+}$ and [**BTT-4**]$^{3+}$ the doublet and quadruplet states are almost degenerate in energy; the quadruplet being more stable for [**BTT-3**]$^{3+}$ by 0.004 eV and the doublet for [**BTT-4**]$^{3+}$ by 0.028 eV. For [**BTT-5**]$^{3+}$ the quadruplet state turned out to be more stable by 0.233 eV. Finally, singlet, triplet and quintuplet states were computed for [**BTT-5**]$^{4+}$. The quintuplet was predicted to be more stable than the triplet by 0.133 eV and the triplet more stable than the singlet by 0.633 eV. Table S1 gathers the Mulliken atomic charges computed for the BTT core and the OMeTPA groups of the different oxidized species of **BTT-3**, **BTT-4** and **BTT-5** in their more stable electronic state.

Table S1. Mulliken atomic charges (in e) computed for the BTT core and the OMeTPA groups of **BTT-3**, **BTT-4** and **BTT-5** in different oxidized states.

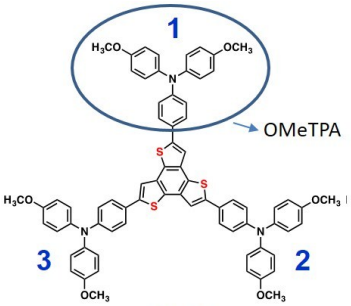

BTT-3

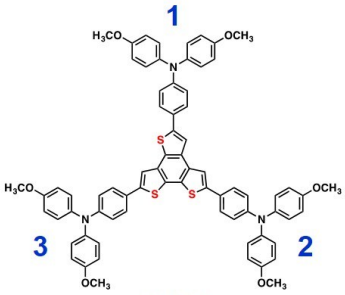

BTT-4

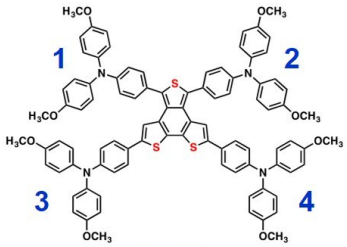

BTT-5

Compound	Neutral	Cation	Dication	Trication	Tetracation
BTT-3					
Core	–0.39	–0.19	–0.08	–0.04	
OMeTPA-1	0.13	0.38	0.69	1.01	
OMeTPA-2	0.13	0.38	0.69	1.01	
OMeTPA-3	0.13	0.43	0.69	1.02	
BTT-4					
Core	–0.39	–0.14	–0.04	–0.01	
OMeTPA1	0.12	0.23	0.90	1.01	
OMeTPA2	0.13	0.50	0.53	1.00	
OMeTPA3	0.14	0.41	0.62	1.01	
BTT-5					
Core	–0.45	–0.15	0.03	–0.07	–0.08
OMeTPA1	0.10	0.26	0.47	0.52	1.03
OMeTPA2	0.10	0.26	0.47	0.51	1.03
OMeTPA3	0.13	0.32	0.51	1.02	1.01
OMeTPA4	0.13	0.32	0.51	1.02	1.01

Figure S4 represents the potential energy surfaces for the neutral and cation states of two molecules (labelled as 1 and 2) involved in a charge transfer process. The intramolecular reorganization energy (λ) consists of two terms related to the geometry relaxation energies of one molecule going from the fully relaxed ground state of the neutral species to the cation state (Figure S4, left) and a neighbouring molecule evolving in the opposite way (Figure S4, right),

$$\lambda = \lambda_1 + \lambda_2 \qquad \text{* MERGEFORMAT (1)}$$

$$\lambda_1 = E\ (M1) - E\ (M1^+) \qquad \text{* MERGEFORMAT (2)}$$

$$\lambda_2 = E\ (M2^+) - E\ (M2) \qquad \text{* MERGEFORMAT (3)}$$

Here, *E*(M1) and *E*(M1$^+$) for molecule 1 are the energies of the positively charged molecule (the cation) at the equilibrium geometry of the neutral molecule and the relaxed cation, respectively, and *E*(M2$^+$) and *E*(M2) for molecule 2 are, accordingly, the energies of the neutral molecule at the equilibrium geometry of the cation and the neutral molecule, respectively.

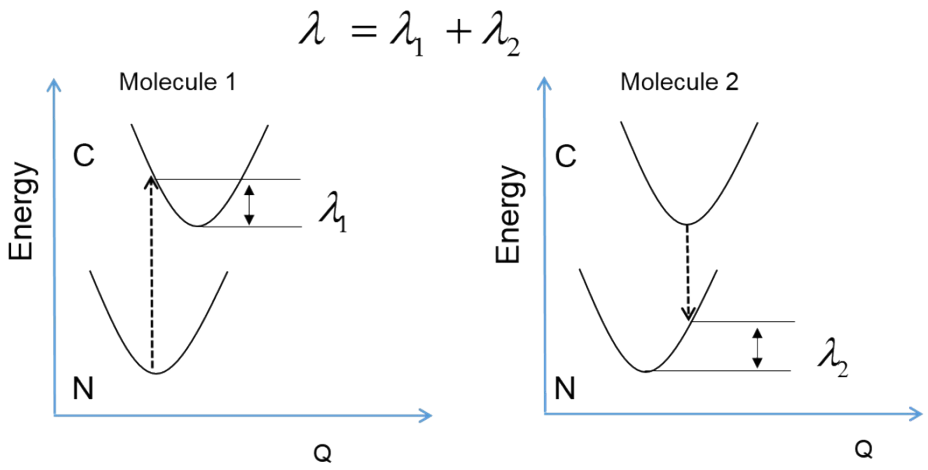

Figure S4. Scheme of the potential energy surfaces of the neutral state (N) and the cation state (C) for two molecules (1 and 2) involved in a charge (hole) transfer process. λ_1 and λ_2 are the two contributions to the total intramolecular reorganization energy (λ).

Table S2 collects the vertical excitation energies (*E*), oscillator strengths (*f*) and electronic descriptions in terms of one-electron molecular orbital excitations calculated for the most first five singlet→singlet ($S_0 \rightarrow S_n$) transitions of **BTT-3**, **BTT-4** and **BTT-5** in CH_2Cl_2 solution. Figure S4 shows the molecular orbitals involved in the $S_0 \rightarrow S_n$ transitions quoted in Table S1.

Table S2. Lowest singlet excited states calculated at the TDDFT B3LYP/6-31G** level for **BTT-3**, **BTT-4** and **BTT-5** in CH_2Cl_2 solution. Vertical excitation energies (*E*), oscillator strengths (*f*) and dominant monoexcitations with contributions (within parentheses) greater than 20%.

Compound	State	*E* (eV/nm)	*f*	Description[a]
BTT-3	S_1	2.86 / 433	1.735	H → L (53)
				H–1 → L+1 (20)
	S_2	2.90 / 428	1.639	H → L+1 (42)
				H–1 → L (24)
	S_3	2.91 / 426	0.023	H–1 → L (56)
				H → L+1 (38)
	S_4	3.03 / 409	0.043	H–1 → L+1 (56)
				H → L (38)
	S_5	3.10 / 400	0.039	H–2 → L (71)
BTT-4	S_1	2.57 / 482	1.531	H → L (97)
	S_2	2.80 / 443	0.757	H–1 → L (91)
	S_3	2.93 / 424	0.162	H–2 → L (83)
	S_4	3.04 / 407	0.579	H → L+1 (81)
	S_5	3.28 / 378	0.220	H–1 → L+1 (90)
BTT-5	S_1	2.37 / 524	1.417	H → L (99)
	S_2	2.67 / 465	0.027	H–1 → L (98)
	S_3	2.75 / 449	0.135	H–2 → L (53)
				H–3 → L (45)
	S_4	2.82 / 440	0.037	H–2 → L (45)
				H–3 → L (54)
	S_5	2.95 / 420	0.008	H → L+1 (95)

[a] H and L denotes HOMO and LUMO, respectively.

[1] Gaussian 09, Revision D.01, M. J. Frisch, G. W. Trucks, H. B. Schlegel, G. E. Scuseria, M. A. Robb, J. R. Cheeseman, G. Scalmani, V. Barone, B. Mennucci, G. A. Petersson, H. Nakatsuji, M. Caricato, X. Li, H. P. Hratchian, A. F. Izmaylov, J. Bloino, G. Zheng, J. L. Sonnenberg, M. Hada, M. Ehara, K. Toyota, R. Fukuda, J. Hasegawa, M. Ishida, T. Nakajima, Y. Honda, O. Kitao, H. Nakai, T. Vreven, J. A. Montgomery, J. E. Peralta, F. Ogliaro, M. Bearpark, J. J. Heyd, E. Brothers, K. N. Kudin, V. N. Staroverov, R. Kobayashi, J. Normand, K. Raghavachari, A. Rendell, J. C. Burant, S. S. Iyengar, J. Tomasi, M. Cossi, N. Rega, J. M. Millam, M. Klene, J. E. Knox, J. B. Cross, V. Bakken, C. Adamo, J. Jaramillo, R. Gomperts, R. E. Stratmann, O. Yazyev, A. J. Austin, R. Cammi, C. Pomelli, J. W. Ochterski, R. L. Martin, K. Morokuma, V. G. Zakrzewski, G. A. Voth, P. Salvador, J. J. Dannenberg, S. Dapprich, A. D. Daniels, Farkas, J. B. Foresman, J. V. Ortiz, J. Cioslowski, D. J. Fox, Gaussian, Inc., Wallingford CT, 2009.

[2] a) C. Lee, W. Yang, R. G. Parr, *Phys. Rev. B* **1988**, *37*, 785-789; b) A. D. Becke, *J. Chem. Phys.* **1993**, *98*, 5648-5652.

[3] M. M. Francl, W. J. Pietro, W. J. Hehre, J. S. Binkley, M. S. Gordon, D. J. Defrees, J. A. Pople, *J. Chem. Phys.* **1982**, *77*, 3654-3665.

[4] a) J. Tomasi, M. Persico, Chem. Rev. 1994, 94, 2027–2094; b) J. Tomasi, B. Mennucci, R. Cammi, Chem. Rev. 2005, 105, 2999–3093; c) C. S. Cramer, D. G. Truhlar, in: Solvent Effects and Chemical Reactivity (Eds.: O. Tapia, J. Bertrán), Kluwer, Dordrecht, The Netherlands, 1996, p. 1–80.

[5] a) M. E. Casida, C. Jamorski, K. C. Casida, D. R. Salahub, *J. Chem. Phys.* **1998**, *108*, 4439-4449; b) C. Jamorski, M. E. Casida, D. R. Salahub, *J. Chem. Phys.* **1996**, *104*, 5134-5147; c) M. Petersilka, U. J. Gossmann, E. K. U. Gross, *Phys. Rev. Lett.* **1996**, *76*, 1212-1215.

[6] http://www.chemcraftprog.com

4. Device preparation

Conductive FTO glass (NSG10) was sequentially cleaned by sonication in a 2 % Helmanex solution and isopropanol for 15 min, respectively. A 30 nm titania blocking layer was applied on the substrates by spraying a solution of titanium diisopropoxide bis(acetylacetonate) in ethanol at 450 °C. For the 200–300 nm mesoporous TiO_2 layer, 30 NR-D titania paste from Dyesol diluted in ethanol (ratio 1:8 by weight) was applied by spin-coating at 2000 rpm for 10 s followed by a sintering step at 500 °C for 20 min. After cooling down the substrates, a Li-treatment was applied by spin-coating 60 µL of a solution of tris(bis(trifluoromethylsulfonyl)imide) (Li-TFSI) in acetonitrile (10mg/mL) onto the mesoporous layer, followed by a sintering step at 500 °C for 10 min to decompose the Li-salt as previously described.[7] The perovskite layers were fabricated by a single step spin-coating procedure reported by Soek et al.[8] For the perovskite precursor solution. 508 mg of PbI_2(TCI), 68 mg PbI_2 (TCI), 180.5 mg of formamidinium iodide (Dyesol) and 20.7 mg of methylammonium bromide (Dyesol) were dissolved in a 1:4 mixture of DMSO:DMF. The perovskite solution was spun at 5000 rpm for 30 s using a ramp of 3000 rpm s^{-1}. 15 s prior to the end of the spin-coating sequence, 100 µL of chlorobenzene were poured onto the spinning substrate. Afterwards, the substrates were transferred onto a heating plate and annealed at 100 °C for 45 min. The hole-transporting materials were applied from solutions in chlorobenzene. Optimized concentrations were found to be 20 mM for **BTT-4** and **BTT-5** and 60 mM for spiro-OMeTAD. Tert-butylpyridine (Tbp), tris(2-(1H-pyrazol-1-yl)-4-tert-butylpyridine)cobalt(III) (FK209) and Li-TFSI were added as additives. Equimolar amounts of additives were added for all hole-transporters: 330 mol% Tbp, 50 mol% Li-TFSI from a 1.8 M stock solution in acetonitrile and 3 mol% FK209 from a 0.25 M stock solution in acetonitrile. The final HTM solutions were spin-coated dynamically onto the perovskite layers at 4000 rpm for 20s. The gold electrodes were deposited by thermal evaporation of 70 nm gold using a shadow mask under high-vacuum conditions.

[7] F. Giordano, A. Abate, J. P. Correa-Baena, M. Saliba, T. Matsui, S. H. Im, S. M. Zakeeruddin, M. K. Nazeeruddin, A. Hagfeldt, M. Graetzel, *Nat. Commun.* **2016**, *7*, 10379.
[8] N. J. Jeon, J. H. Noh, Y. C. Kim, W. S. Yang, S. Ryu, S. I. Seok, *Nat. Mater.* **2014**, *13*, 897.

5. Solar cell characterization

The photovoltaic device performance was analyzed using a VeraSol LED solar simulator (Newport) producing 1 sun AM 1.5 G (100 W cm^{-2}) sunlight. Current density-voltage curves were measured in air with a potentiostat (Keithley). The light intensity was calibrated with an NREL certified KG5 filtered Si reference diode. The solar cells were masked with a metal aperture of 0.16 cm^2 to define the active area. The current-voltage curves were recorded scanning at 20 mV s^{-1}.

5.1 Spiro OMeTAD reference cell

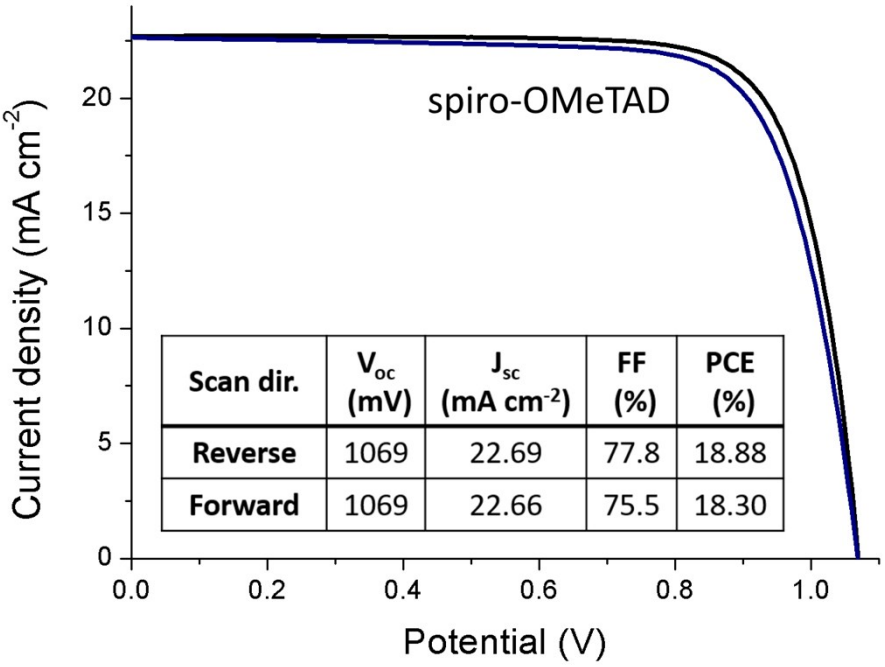

Scan dir.	V_{oc} (mV)	J_{sc} (mA cm^{-2})	FF (%)	PCE (%)
Reverse	1069	22.69	77.8	18.88
Forward	1069	22.66	75.5	18.30

Figure S5. Reference cell fabricated using spiro-OMeTAD as HTM.

6. SEM images

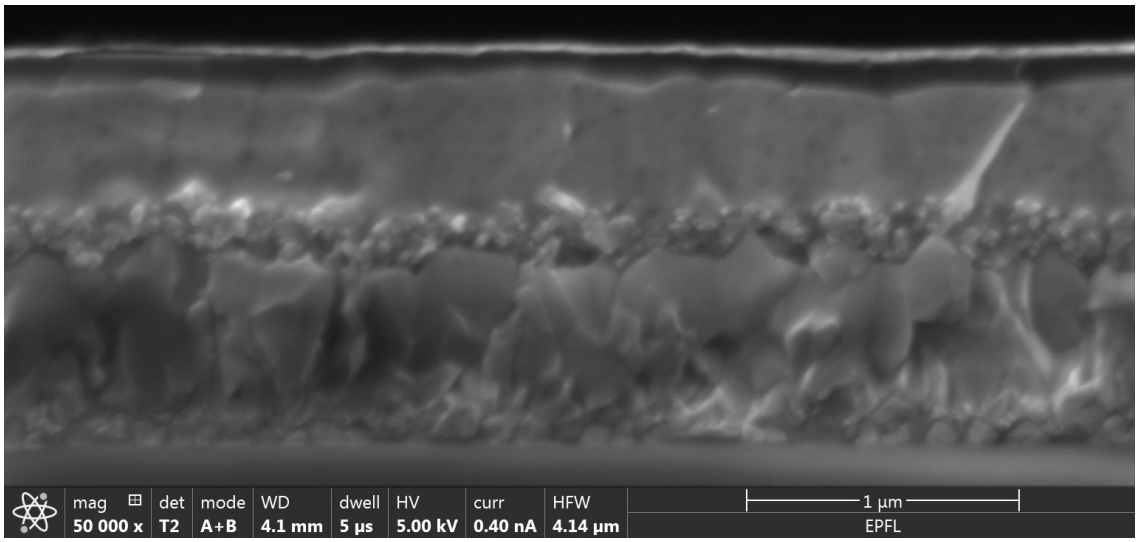

Figure S6. SEM cross-sectional image of a PSC device fabricated using **BTT-5** as HTM.

7. Supplementary figures

7.1. TGA and DSC

7.1.1 Thermogravimetric Analysis (TGA)

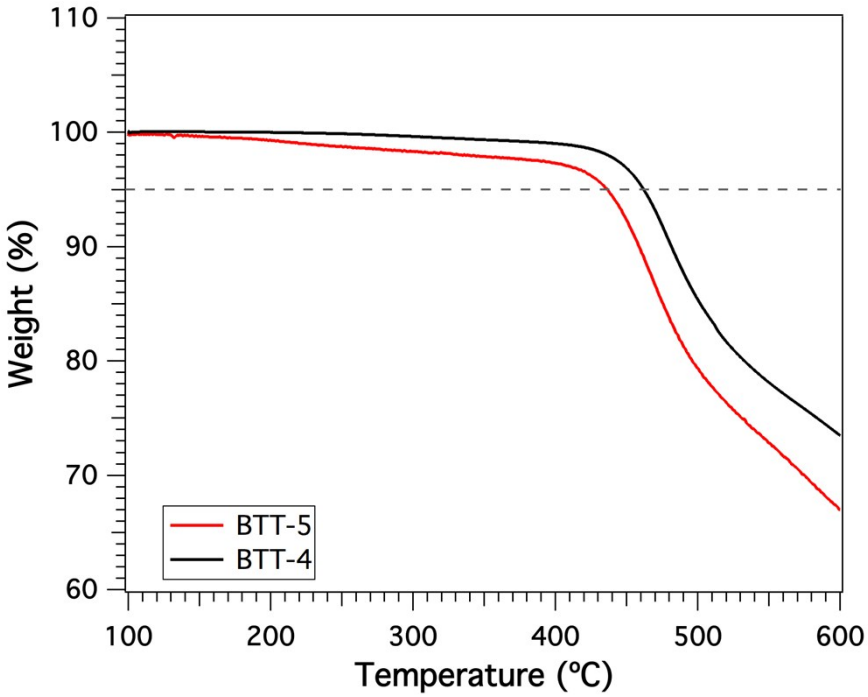

Figure S7. Thermogravimetric analysis of **BTT-4** and **BTT-5** at a scan rate of 10 °C min^{-1}.

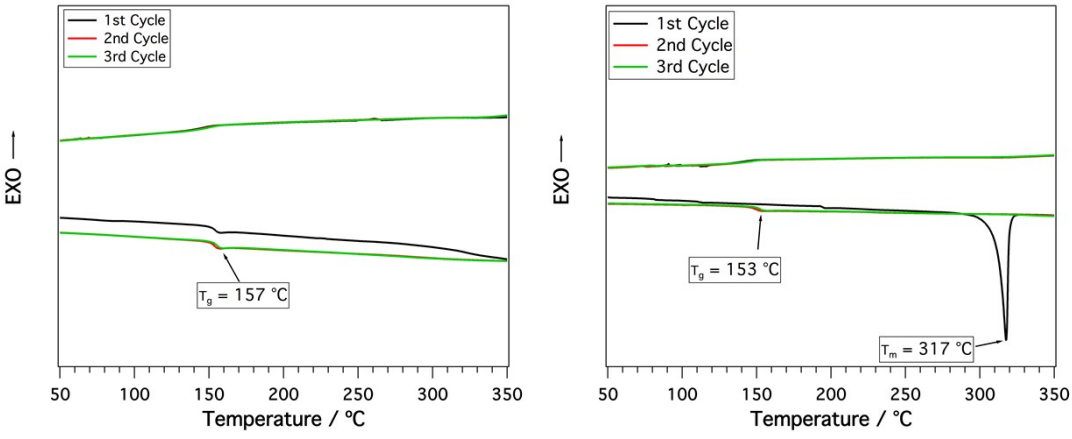

Figure S8. DSC of **BTT-4** (left) and **BTT-5** (right) and at a scan rate of 20 °C min^{-1}.

7.2. NMR, MS

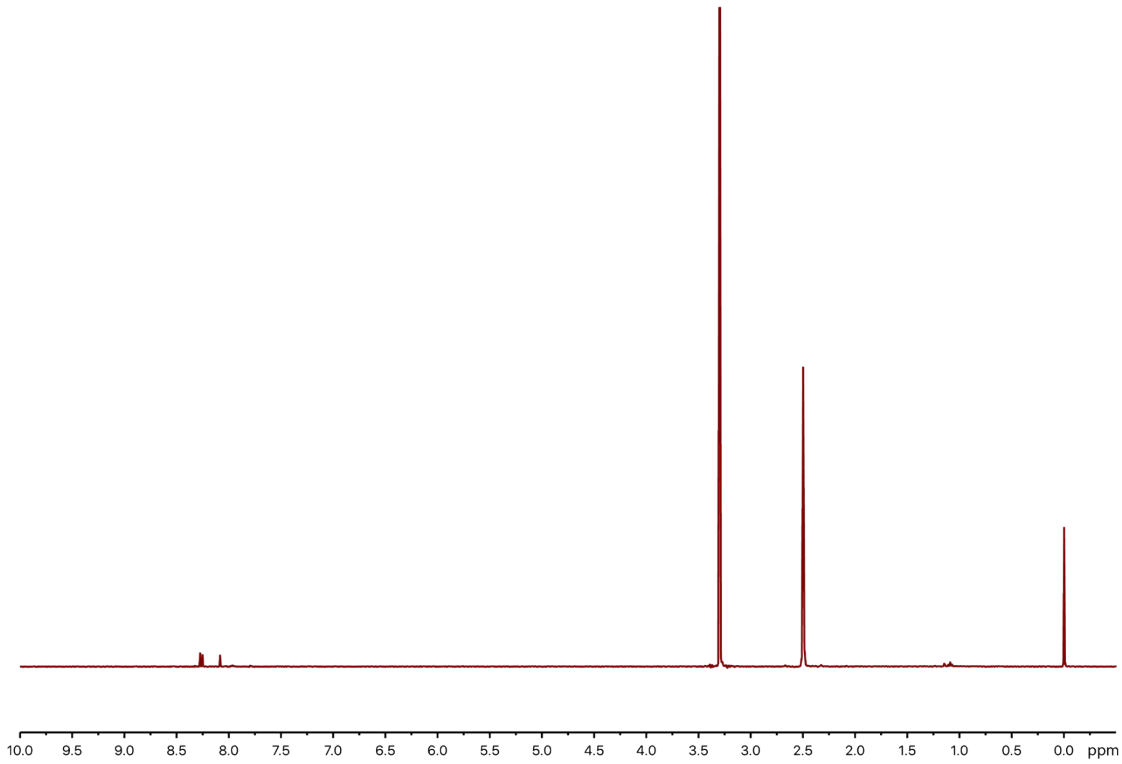

Figure S9. ^{1}H NMR (400 MHz, DMSO-d_6, 298 K) of 2,5,8-tribromobenzo[1,2-*b*:3,4-*b*':6,5-*b*'']trithiophene **(3).**

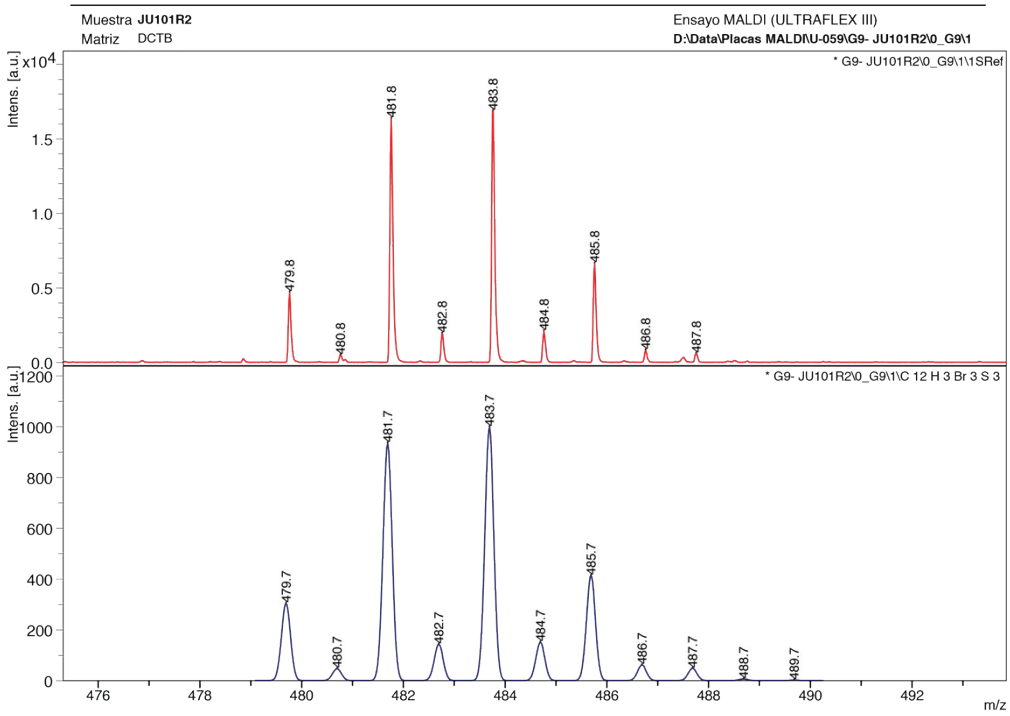

Figure S10. MALDI-TOF mass spectrum of 2,5,8-tribromobenzo[1,2-*b*:3,4-*b*':6,5-*b*'']trithiophene (**3**).

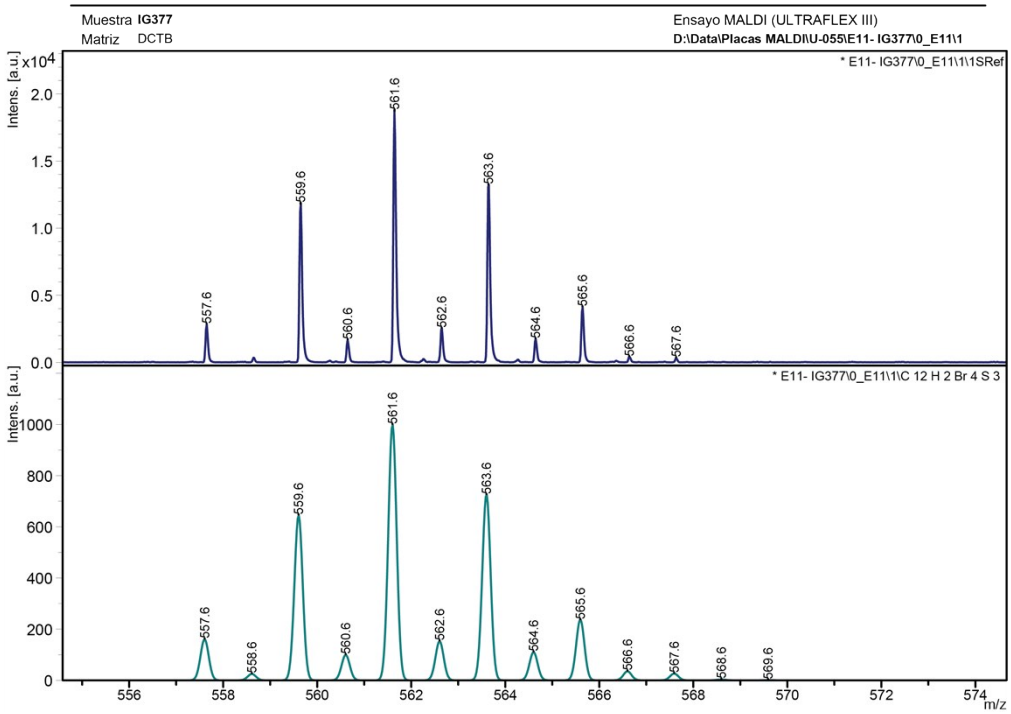

Figure S11. MALDI-TOF mass spectrum of 2,4,6,8-tetrabromobenzo[1,2-*b*:6,5-*b'*:3,4-*c''*]trithiophene (**6**).

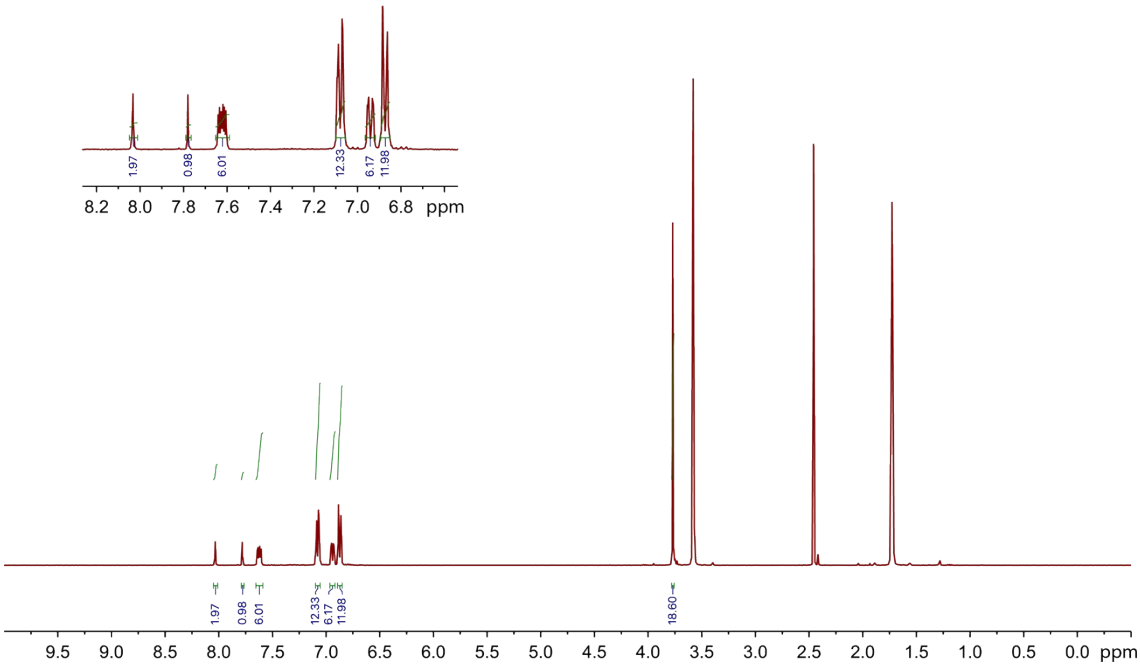

Figure S12. ^{1}H NMR (400 MHz, THF-d_8, 298 K) of **BTT-4**.

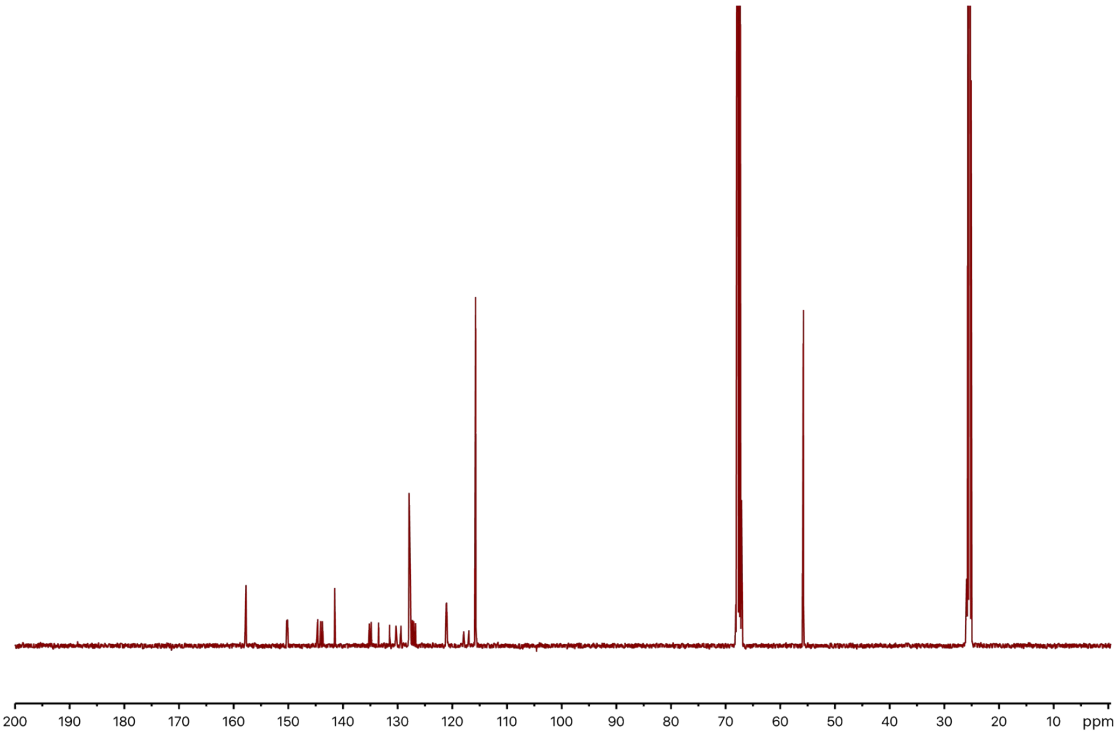

Figure S13. ^{13}C NMR (100 MHz, $CDCl_3$, 298 K) of **BTT-4**.

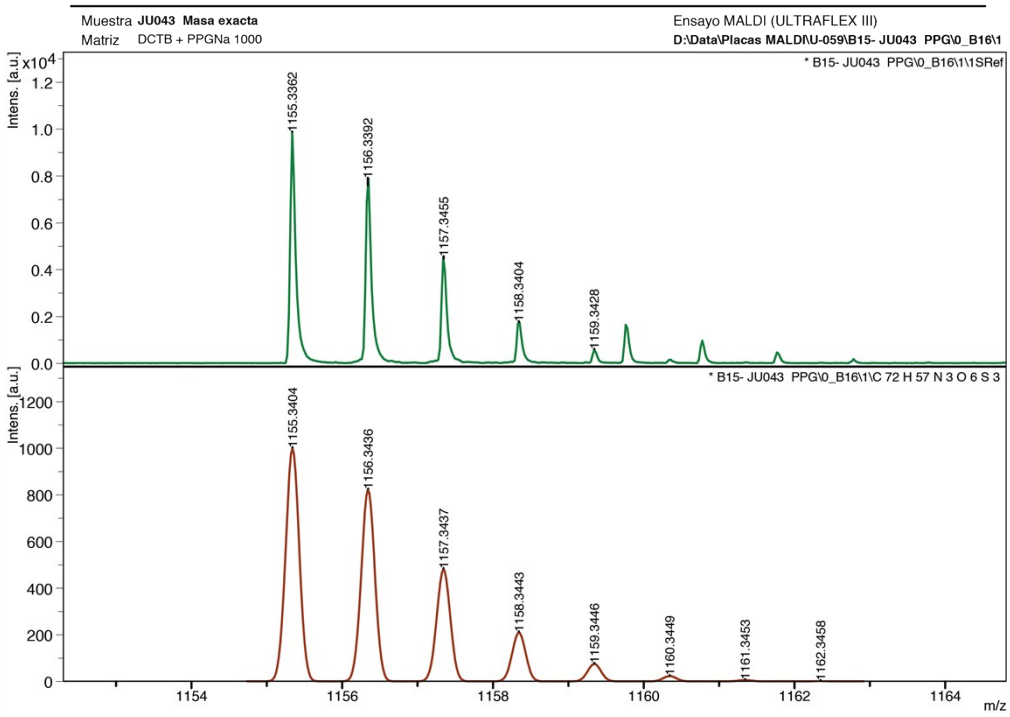

Figure S14. HR-MALDI-TOF mass spectrum of **BTT-4.**

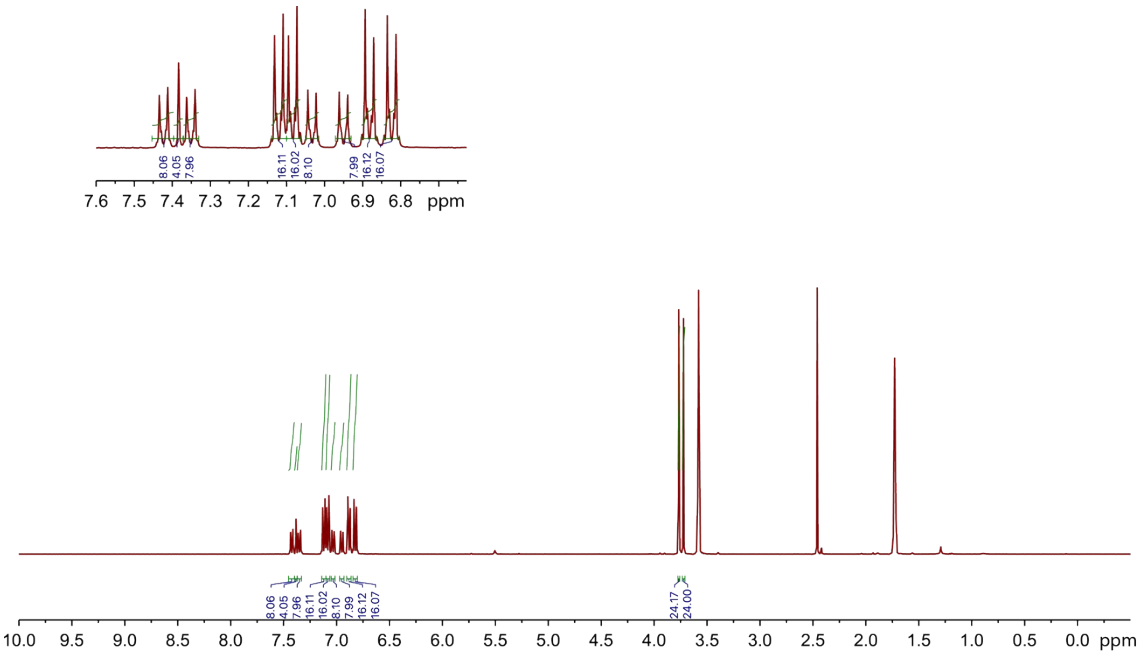

Figure S15. ^{1}H NMR (400 MHz, THF-d_8, 298 K) of **BTT-5**.

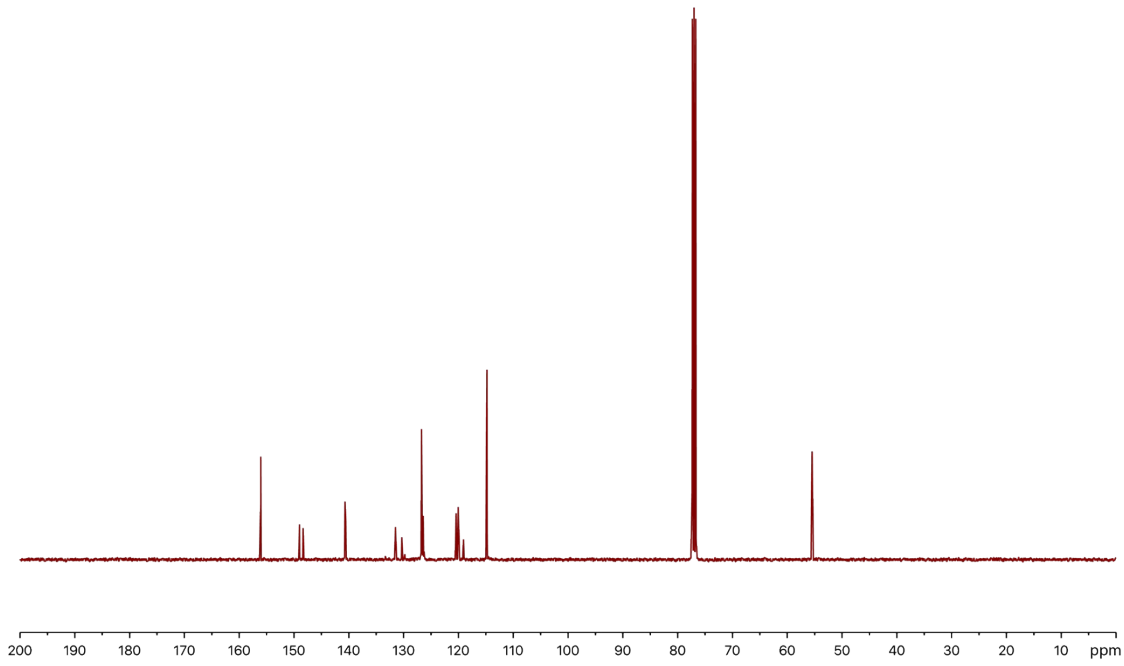

Figure S16. ^{13}C NMR (100 MHz, $CDCl_3$, 298 K) of **BTT-5**.

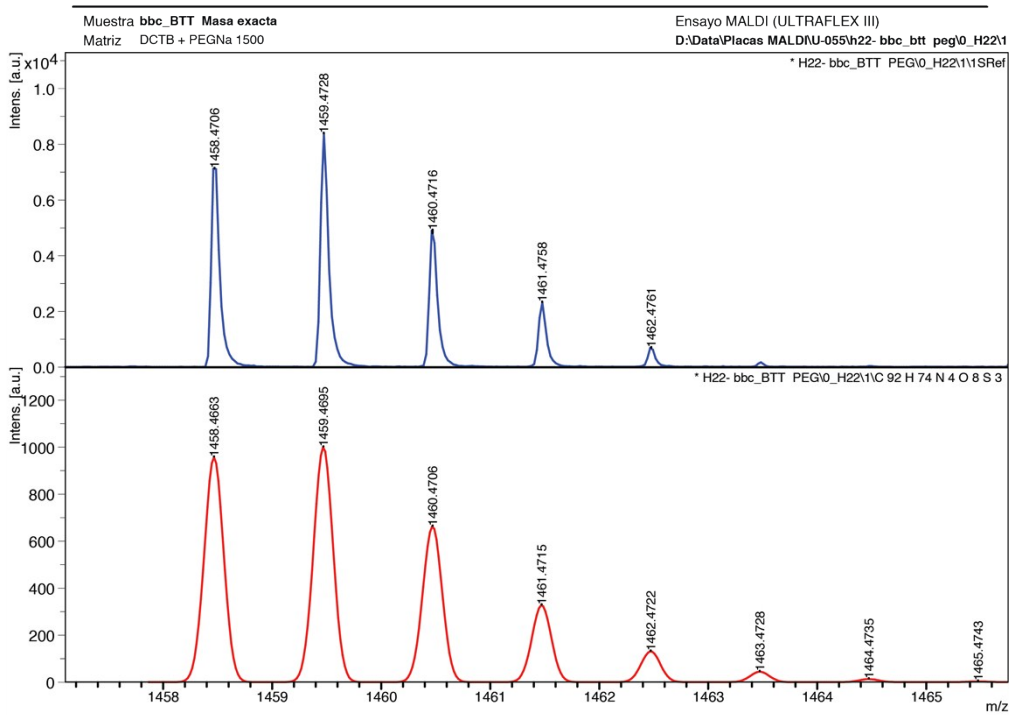

Figure S17. HR-MALDI-TOF mass spectrum of **BTT-5.**